Efficient Parameterization Strategies for Optimizing Sub-Wavelength Focusing Structures

Felix Huber[1], Fabian Wein[2], Florian Toth[1]

[1] *Institute of Mechanics and Mechatronics, 1060 Vienna, Austria, Email: felix.huber@tuwien.ac.at*

[2] *Department of Mathematics, 91058 Erlangen, Germany*

Motivation

In the field of acoustic topology optimization, there has recently been growing interest in optimizing macrostructures for focusing devices such as the sonic black holes (SBHs) by Mousavi, Berggren, Hägg, *et al.* [1], which are the airborne equivalents to structural acoustic black holes (ABHs) [2]. Acoustic wave propagation problems are inherently sensitive, which complicates the search for black-and-white solutions. They require advanced filters or parameterization to obtain good convergence and a useful design.

In this contribution, we explore density-based parameterization methods, starting with the classic solid isotropic material with penalization (SIMP) approach, in which practically every finite element mesh cell is an optimization variable [3]. In contrast, the contemporary feature-mapping model uses high-level geometric objects as parameters. Here, we compare a classical feature-mapping approach with linked rounded bars [4] with a shape-optimization variant [5]. Both mapping approaches significantly reduce the number of optimization parameters in the system, thereby increasing regularization. Although the method is mathematically more complex, the increased controllability is a useful tool for design control, e.g., for manufacturability via 3D printing, and the inherently black-and-white designs are particularly interesting for sub-wavelength optimization.

Modelling

To optimize the material distribution, we first have to establish a method of modelling the acoustic wave propagation. We start with the Helmholtz equation for inhomogenous media

$$-\omega^2\kappa^{-1}p - \boldsymbol{\nabla}\cdot\left(\rho_0^{-1}\boldsymbol{\nabla}p\right) = 0 \qquad \text{in } \Omega, \tag{1}$$

with angular frequency ω and unknown pressure field $p \in \Omega$. The material is described via bulk modulus κ and material density ρ_0. To model the setup for our numerical study, shown in Fig. 3, we need to define the boundary conditions (BCs)

$$\left.\frac{\partial p}{\partial \mathbf{n}}\right|_{\Gamma_{\text{exc}}} = -j\omega(c_o^{-1}p + \rho_0 v_{\text{n}}), \tag{2}$$

$$\left.\frac{\partial p}{\partial \mathbf{n}}\right|_{\Gamma_{\text{abc}}} = -j\omega c_o^{-1}p, \tag{3}$$

with excitation normal velocity v_{n} and absorbing boundary condition (ABC) terms on both ends of the waveguide. The combination of Neumann BC and ABC on Γ_{exc} acts as transparent excitation. Using the finite element method (FEM), the acoustic model given in Eqs. (1) to (3) is dicretized on a grid and transformed into a discrete system of the structure

$$\underbrace{\left(-\omega^2\mathbf{M} + j\omega\mathbf{C} + \mathbf{K}\right)}_{\mathbf{S}}\mathbf{p} = \mathbf{f}. \tag{4}$$

The different contributions of mass in $\mathbf{M}$, ABCs in $\mathbf{C}$ and stiffness in $\mathbf{K}$ are combined into the system matrix $\mathbf{S}$ [6].

Parameterization

To enable the choice of material or no material, for a constant FEM grid, we introduce an element-based physical pseudo density $\widetilde{\rho}_e$, which is used to scale the material parameters inversely; resulting in unchanged material for $\widetilde{\rho}_e = 1$ and very stiff material for $\widetilde{\rho}_e \approx 0$. This approach can be nicely integrated in the assembly of the FEM model from Eq. (4), using

$$\mathbf{S} = \bigwedge_{e=1}^{E} \begin{cases} \mathbf{S}_e & \forall e \in \Omega_{\text{acou}} \\ \mathbf{S}_e\widetilde{\rho}_e & \forall e \in \Omega_{\text{opt}}. \end{cases} \tag{5}$$

with the assembly operator $\bigwedge$ taken from [6].

To the widespread SIMP approach, the parameters of the optimization are the pseudo-desnities themselves, which we collect in the parameter vector

$$\boldsymbol{\rho} = \begin{bmatrix}\rho_1 & \rho_2 & \dots & \rho_E\end{bmatrix}^{\intercal}. \tag{6}$$

We map them to the physical pseudo-densities via a radius-based density filter and penalization [3]; however, for wave propagation problems, we neglect penalization and rather choose projection [7] to achieve a binary design. The procedure is summarized as

$$\widetilde{\boldsymbol{\rho}}(\boldsymbol{\rho}; R, \beta) = H(\bar{\boldsymbol{\rho}}; \beta) = H(\mu(\boldsymbol{\rho}; R); \beta), \tag{7}$$

with the projection function H with steepness paramter β and radius based density filter μ with radius paramter R. The advantages of this method are its simplicity and low regularization (high degrees of freedom (DOFs)), but the latter can pose problems when you want to enforce specific properties on the design.

This is precisely where feature-mapping methods come in handy. We introduce high level features with a paramter set $\dim(\boldsymbol{\chi}) \ll \dim\boldsymbol{\rho}$. Because we want to use the same FEM grid and physical parameterization as in Eq. (5), we need a mapping from feature parameters $\boldsymbol{\chi}$ to physical pseudo densities $\widetilde{\boldsymbol{\rho}}$, which usually follows a three-step process.

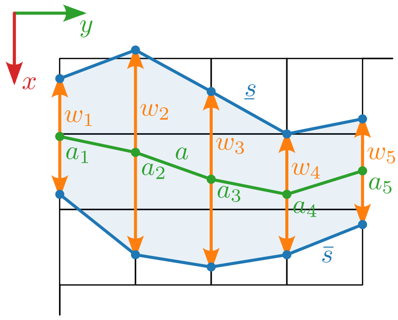

Figure 1: SM uses midpoints a and widths w, aligned with the FEM grid, to parameterize the feature boundaries.

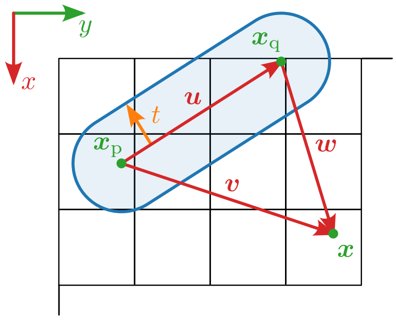

Figure 2: FM uses startpoint $\mathbf{x}_p$, endpoint $\mathbf{x}_q$ and width t to parameterize the feature boundaries. The distance function is computed via the helper vectors $\mathbf{u}$, $\mathbf{v}$ and $\mathbf{w}$.

1. Define a differentiable scalar minimum distance function to the feature edges $d(\mathbf{x};\boldsymbol{\chi})$, which becomes negative inside the feature.
2. Project this distance function with $H(d;\beta)$ to achieve a scaling suitable for pseudo-densities, which is, however, still continuous.
3. Numerically integrate this field over each element, to obtain the respective physical pseudo-density $\widetilde{\rho}_e$.

The procedure is summarized as

$$\widetilde{\boldsymbol{\rho}}(\boldsymbol{\chi};\beta) = \sum_{k=1}^{I} H(d(\mathbf{x}_k;\boldsymbol{\chi});\beta). \tag{8}$$

The full procedure is differentiable, which allows the computation of gradients with respect to the parameters and the use of the same optimizers as in SIMP. For more details on feature-mapping methods, we refer to the review paper [8].

The first variation of the feature-mapping approach considered in this work is shape-mapping (SM) [5]. The shapes in this method are linear splines, with one dimension aligned to the nodes of the FEM grid. For the other dimension, the spline points are defined via midpoints a_i and widths w_j collected in the parameter vector

$$\boldsymbol{\chi} = \begin{bmatrix} a_1 & a_2 & \dots & a_{N_y} & w_1 & w_2 & \dots & w_{N_y} \end{bmatrix}^\intercal, \tag{9}$$

with the number of nodes in y-direction N_y. To illustrate how these shapes look like, we provide a sketch in Fig. 1. The SM approach follows the same procedure introduced in Eq. (8). To obtain a continous distance function we have to linearly interpolate between the base points of the splines, which yields the profile functions $\underline{s}(y,\boldsymbol{\chi})$ and $\bar{s}(y,\boldsymbol{\chi})$, as well as the midpoints $a(y,\boldsymbol{\chi})$. The distance function follows as

$$d(\mathbf{x},\boldsymbol{\chi}) = \begin{cases} \underline{s}(y,\boldsymbol{\chi}) - x & \text{if } x \leq a(y,\boldsymbol{\chi}) \\ x - \bar{s}(y,\boldsymbol{\chi}) & \text{otherwise.} \end{cases}$$

For shape mapping, we use Heaviside-type projection, similar to the projection used in the SIMP method,

$$H_\mathrm{s}(\mathbf{x},\boldsymbol{\chi};\beta) = \frac{1-\rho_\mathrm{min}}{e^{\beta d(\mathbf{x},\boldsymbol{\chi})}+1} + \rho_\mathrm{min}, \tag{10}$$

with a minimum pseudo-density of $\rho_\mathrm{min} = 1\times10^{-9}$. For a more detailed discussion of the method, the combination of several profiles and the respective gradients, we refer to the introductory paper [5].

The second studied method is the round-capped-bar parameterization [4]. As the name implies, the features consist of bars, with defined start- and endpoint, $\mathbf{x}_p$ and $\mathbf{x}_q$, and a thickness t, illustrated in Fig. 2. The ends are closed with semicircles to simplify the distance function. This method has a very low parameter count, resulting in the parameter vector

$$\boldsymbol{\chi} = \begin{bmatrix} \mathbf{x}_p^\intercal & \mathbf{x}_q^\intercal & t \end{bmatrix}^\intercal, \tag{11}$$

Because of its direct applicability in structural mechanics and resulting wide usage, we will refer to it as feature-mapping (FM). We derive the mathematical formulation from the basic concept in Eq. (8), starting with the distance function

$$d_\mathrm{f}(\mathbf{x},\boldsymbol{\chi}) = \begin{cases} \|\mathbf{v}\| - t & \text{if } \mathbf{u}\cdot\mathbf{v} \leq 0 \\ \|\mathbf{w}\| - t & \text{if } \mathbf{u}\cdot\mathbf{v} \geq \mathbf{u}\cdot\mathbf{u} \\ \|\mathbf{u}\times\mathbf{v}\| \frac{1}{\|\mathbf{u}\|} - t & \text{otherwise,} \end{cases} \tag{12}$$

with utility vectors

$$\mathbf{u} = \mathbf{x}_\mathrm{q} - \mathbf{x}_\mathrm{p}, \quad \mathbf{v} = \mathbf{x} - \mathbf{x}_\mathrm{p}, \quad \mathbf{w} = \mathbf{x} - \mathbf{x}_\mathrm{q}. \tag{13}$$

The different parts of the distance function cover the different cases, depending on which feature edge the point of interest $\mathbf{x}$ is closest to. For the projection of the distance function, we use a cubic spline step

$$H_\mathrm{f}(\mathbf{x},\boldsymbol{\chi}_{\mathrm{f},i};h) = \begin{cases} 1 & \text{if } d_\mathrm{f} < -h \\ \sigma(d_\mathrm{f}(\mathbf{x},\boldsymbol{\chi}_{\mathrm{f},i}),h) & \text{if } -h \leq d_\mathrm{f} \leq h \\ \rho_\mathrm{min} & \text{otherwise,} \end{cases} \tag{14}$$

with

$$\sigma = \frac{3(1-\rho_\mathrm{min})}{4}\left(\frac{d_\mathrm{f}}{h} - \frac{d_\mathrm{f}^3}{3h^3}\right) + \frac{1+\rho_\mathrm{min}}{2}. \tag{15}$$

This has the benefits of precise step width control and efficient computation, making this formulation superior to the Heaviside projection in many applications.

Because a single bar is often not enough to achieve an optimal design, they are usually used in combination, subject to certain constraints. In this study, we used three

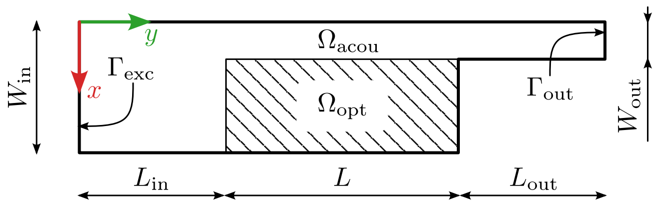

Figure 3: Sketch of the simulation setup, with air domain Ω_{acou}, optimization domain Ω_{opt}, and the boundaries Γ_{exc} and Γ_{out} set to mimic an infinite baffle with invisible excitation.

connected bars with their thicknesses linked, resulting in a total of 9 parameters. A more detailed discussion on the method, especially on the combination of shapes and differentiability, can be found in the original publication [4].

Broadband Objective

To conduct optimization, one needs to define a scalar functional to minimize. We aim to optimize structures for wave focusing; therefore, our cost function is proportional to the reflected wave amplitude, which we want to minimize. Note that, for lossless acoustics, this is equivalent to maximizing the outlet pressure, but we found the first approach converged faster in our example.

The cost function is defined as

$$J \approx (\mathbf{p} - p_{\text{I}})^{\intercal} \mathbf{L} (\mathbf{p} - p_{\text{I}})^{*}, \tag{16}$$

with the DOFs at the input Γ_{exc} selected with the surface-weighted diagonal selector matrix $\mathbf{L}$. In Eq. (16), we subtract p_{I} from the totaö pressure at the output nodes, which is the incident wave pressure caused by the excitation, computed as

$$p_{\text{I}} = \frac{1}{2}\rho_0 c_0 v_{\text{n}} \qquad \text{on } \Gamma_{\text{exc}}. \tag{17}$$

This concept is a cheap wave-decomposition method that allows us to consider only backward-propagating waves. To enable multi-frequency optimization, we use the arithmetic mean of the cost functions across several frequencies. This is a simple approach, but of course it requires solving the FEM system for each optimization frequency.

Numerical Study

In this work, we test different feature-mapping variants against the classic SIMP approach, with special emphasis on wave-focusing applications in SBH-type devices, where the wavelengths significantly exceed the size of the focusing structure. Therefore, we use the setup shown in Fig. 3, a width step from $W_{\text{in}} = 25\,\text{mm}$ to $W_{\text{out}} = 5\,\text{mm}$ in a planar waveguide. The transistion zone has a maximum length of $L = 50\,\text{mm}$, with equal length for inlet L_{in} and outlet L_{out}. We discretize the model with a regular grid, using 50 quadrilateral linear elements in the width direction, resulting in 300 elements in the length direction for the total domain. The target frequency range extends from 1 kHz to 3 kHz using 5 equally spaced frequencies. For this range, we are well below the waveguide's off-axis modes, ensuring plane-wave propagation.

The results of these optimization runs are shown in Fig. 4, where we show the physical pseudo-density fields and the respective transmission coefficients for each method. We observe that all three designs show the same topological properties, but SIMP and SM form a three-cavity structure, while FM has one cavity and then a gradual width change towards the output. This is clearly a result of the strong regularization in FM, which uses only 9 parameters.

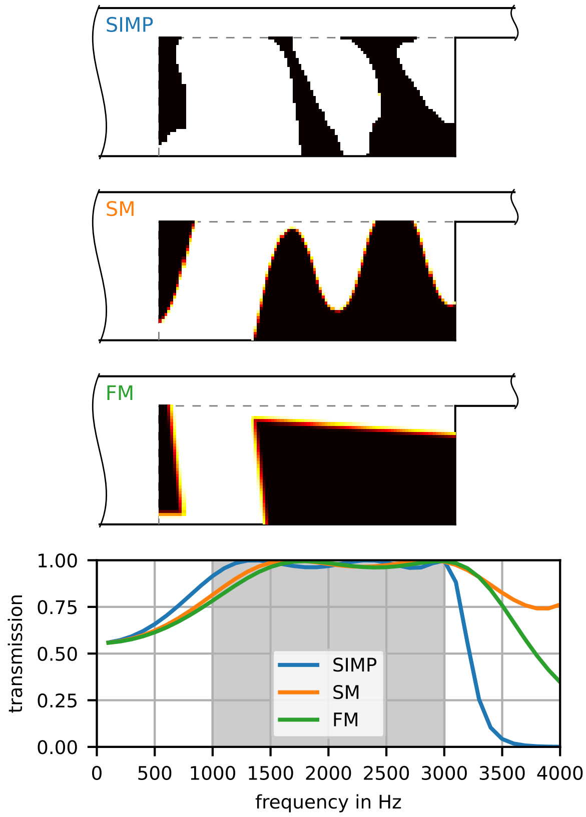

Figure 4: Resulting density fields for the three tested methods (top) and their respective transmission coefficients over frequency of the thresholded design.

Despite the significant differences in regularization, all designs achieved globally optimal transmission across most of the target frequency range. In the lower frequency range, the SIMP design is slightly better, indicating that a good low-frequency design needs more design freedom than the low parameter counts of the other designs allow. For high frequencies, all designs perform well, with the feature-mapping methods rolling off more smoothly. One significant observation is that the three-bar parameterization, despite its simplicity, performs very closely to the two other, more complex shapes, indicating that the multi-chamber design might not be so impactful as believed.

The studies were conducted on an Xeon E5-2640-based server on four logical cores using the open-source FEM software openCFS [9]. Despite its extensive simulation capabilities, openCFS also implements many optimization features, which we extended for this study. To solve the optimization problem, we used the sparse nonlinear optimizer (SNOPT) [10], because it proved to be most stable for our studies.

The benchmark results of our numerical studies are presented in Fig. 5 for each parameterization method. SIMP converged the slowest, taking 650 s for about 300 iterations. SM took 378 s and also less iterations. The commonality between the two is the use of a Heaviside-type projection, for which we achieved good results by starting with a low β-factor for good gradient conditioning and steadily increasing it to force the solution to be binary. To make this process easy on the optimizer, we keep the β-factor constant until we converge with a Karush-Kuhn-Tucker (KKT) of 1×10^{-6} or reach the 500-iterations limit. Then we restart the optimization with an exponentially stepped β-factor, warm-started with the previous design. We repeat this process for a total of ten steps. The round-capped-bar FM approach uses a polynomial projection function that obviates this process. Here we can directly use the target step width of $t = 1\,\text{mm}$ ad see great convergence in only 53 s.

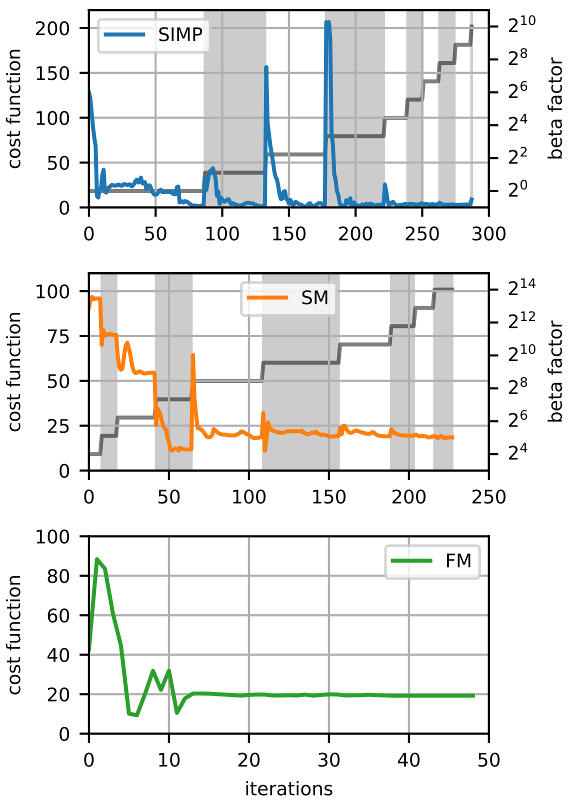

Figure 5: Benchmark results on four logical cores of an Xeon E5-2640. Cost function over iterations for each method; for the first two, we plot the stepped β-factor logarithmically on the right, with the constant regions indicated by a gray background.

Conclusion and Outlook

The tested parameterization approaches enabled the synthesis of drastically simplified designs, due to their high regularization. On the contrary, this drastic reduction in parameters also slightly reduced the low-frequency focusing of the structures. Computationally, both feature-mapping approaches performed better than the full parameter SIMP model. Furthermore, round-capped-bar FM significantly outperformed SM, mainly due to the robust polynomial step projection function. We hope this study will be helpful for future research in acoustic topology optimization, and encourage the reader to try one of the tested feature-mapping approaches.

References

[1] A. Mousavi, M. Berggren, L. Hägg, and E. Wadbro, "Topology optimization of a waveguide acoustic black hole for enhanced wave focusing," en, *The Journal of the Acoustical Society of America*, vol. 155, no. 1, pp. 742–756, Jan. 1, 2024, ISSN: 0001-4966. DOI: 10.1121/10.0024470.

[2] A. Pelat, F. Gautier, S. C. Conlon, and F. Semperlotti, "The acoustic black hole: A review of theory and applications," en, *Journal of Sound and Vibration*, vol. 476, p. 115 316, Jun. 2020, ISSN: 0022460X. DOI: 10.1016/j.jsv.2020.115316.

[3] M. P. Bendsøe, "Optimal shape design as a material distribution problem," en, *Structural Optimization*, vol. 1, no. 4, pp. 193–202, Dec. 1989, ISSN: 0934-4373, 1615-1488. DOI: 10.1007/BF01650949.

[4] J. A. Norato, B. K. Bell, and D. A. Tortorelli, "A geometry projection method for continuum-based topology optimization with discrete elements," en, *Computer Methods in Applied Mechanics and Engineering*, vol. 293, pp. 306–327, Aug. 2015, ISSN: 00457825. DOI: 10.1016/j.cma.2015.05.005.

[5] F. Wein and M. Stingl, "A combined parametric shape optimization and ersatz material approach," en, *Structural and Multidisciplinary Optimization*, vol. 57, no. 3, pp. 1297–1315, Mar. 2018, ISSN: 1615-147X, 1615-1488. DOI: 10.1007/s00158-017-1812-3.

[6] M. Kaltenbacher, *Numerical Simulation of Mechatronic Sensors and Actuators*, en. Berlin, Heidelberg: Springer Berlin Heidelberg, 2007, ISBN: 978-3-540-71359-3. DOI: 10.1007/978-3-540-71360-9.

[7] J. K. Guest, J. H. Prévost, and T. Belytschko, "Achieving minimum length scale in topology optimization using nodal design variables and projection functions," en, *International Journal for Numerical Methods in Engineering*, vol. 61, no. 2, pp. 238–254, Sep. 14, 2004, ISSN: 0029-5981, 1097-0207. DOI: 10.1002/nme.1064.

[8] F. Wein, P. D. Dunning, and J. A. Norato, "A review on feature-mapping methods for structural optimization," en, *Structural and Multidisciplinary Optimization*, vol. 62, no. 4, pp. 1597–1638, Oct. 2020, ISSN: 1615-147X, 1615-1488. DOI: 10.1007/s00158-020-02649-6.

[9] openCFS, *Coupled Field Simulation*, https://gitlab.com/openCFS/cfs, 2025.

[10] P. E. Gill, W. Murray, and M. A. Saunders, "SNOPT: An SQP Algorithm for Large-Scale Constrained Optimization," en, *SIAM Review*, vol. 47, no. 1, pp. 99–131, Jan. 2005, ISSN: 0036-1445, 1095-7200. DOI: 10.1137/S0036144504446096.